Q. J. R. Meteorol. Soc. (2006), **132**, pp. 447–465 doi: 10.1256/qj.05.05

On the nonlinear interaction between global teleconnection patterns

By V. N. KHOKHLOV[1]*, A. V. GLUSHKOV[2] and N. S. LOBODA[1]

[1]*Odessa State Environmental University, Ukraine*
[2]*Innovative Geosciences Research Centre, Ukraine*

(Received 13 January 2005; revised 26 September 2005)

SUMMARY

Processes of nonlinear interaction between teleconnection patterns are addressed. Evidence of chaotic behaviour for the relationship between the Arctic Oscillation (AO), the Southern Oscillation (SO), and the Antarctic Oscillation (AAO) is examined using cross-redundancy and Granger causality. The analysis is carried out for three epochs of the twentieth century, during which different trends of global temperature were observed. To study the influence of low-frequency variations, a wavelet decomposition is applied. Presented results display many well-known features of feedbacks between climate change and observed trends in the indices of teleconnection patterns. By using wavelet detail components, some behaviour is revealed as being particularly pure. At the same time, some findings require considerable further work, especially the apparent nonlinear interaction between the AO and the AAO. Our results are encouraging for the prospects of a useful model describing climate changes at the decadal and centurial time-scales.

KEYWORDS: Cross-redundancy Granger causality Teleconnection Wavelet decomposition

1. INTRODUCTION

The temporal variations of global temperature (and some other meteorological values, e.g. precipitation) during the last 150 years show the oscillations and intermittency of the climate and to some extent its variations over longer periods. This pattern gives the impression of being chaotic and brings to mind the behaviour of those dynamic systems which (in the modern theory of chaos) evolve on complex-structured limit sets present in their phase spaces and have come to be known as 'strange attractors'. This concept was introduced in meteorology by Lorenz (1963, 1970). In light of the above, the theory of climate variation ought to be the statistical dynamics of the climate system. Obviously, the construction of such a theory cannot be entrusted to geography—the science that had incorporated climatology up to the 1960s—and ought to be given over to physics. This is especially true because the study of climate in the past and present increasingly depends on physical approaches. In addition, the climate system cannot be confined to the atmosphere alone because the atmosphere is not self-sufficient: its instantaneous state does not determine its further evolution. The climate system must include other layers of the Earth, which interact with the atmosphere. First of all, this includes oceans and seas, and then the upper active layer of solid earth—mainly the land. Moreover, components of the climate system like the atmosphere and oceans exhibit some coherent variability.

The main source of energy for the processes in the Earth climate system is incident solar flux. Its intensity at Earth's mean distance from the Sun, according to both terrestrial and extraterrestrial measurements, is equal to 1360 ± 20 W m^{-2}. However, the solar forcing of climate variations on the decadal and centurial time-scales is too small. Oh *et al.* (2003) showed that the solar irradiance variations due to the well-known 11-year Schwabe (sunspot) and the 80–90-year Gleissberg cycles amount to 1.5 W m^{-2} and 2.25 W m^{-2} respectively. Thus it is impossible to consider solar forcing as the modulator of climate changes on the aforementioned time-scales.

* Corresponding author: Hydrometeorological Institute, Odessa State Environmental University, 15 Lvovskaya str., 65016 Odessa, Ukraine. e-mail: vkhokhlov@ukr.net

Modern numerical models utilize mainly two approaches allowing the physical interpretation of the observed climate variations: the greenhouse forcing of the climate system (see e.g. Monahan *et al.* 2000; Voss and Mikolajewitcz 2001) and the response of the climatic system to tropical Pacific sea surface temperature (SST) anomalies (see e.g. Hannachi 2001; Hurrell *et al.* 2004). In the latter case, *per se*, the response of the global coupled atmosphere–ocean system to the El Niño–Southern Oscillation (ENSO) events is modelled. The ENSO itself is a dynamical system of the coherently varying atmosphere and ocean, as well as one of the most prominent global teleconnection patterns. Other main teleconnection patterns such as the North Atlantic Oscillation (NAO) and the Pacific North American pattern (PNA), as well as the so-called annular modes—the Arctic Oscillation (AO) and the Antarctic Oscillation (AAO)—possess also the ability to represent the atmosphere–ocean (and, in some cases, the atmosphere–land) interaction.

This remarkable feature of the teleconnection patterns allows us to use the time series of their indices as an integrated indicator for the climate variations over extensive areas of the Earth. Moreover, it is well known that the ENSO affects not only the tropical Pacific Ocean, but also other regions. Thus, the forecast for the particular phase of oscillation on decadal and centurial time-scales allows us to increase the reliability of the forecast of regional climate change.

Another feature of the main teleconnection patterns is the interaction between particular oscillations. This interaction appears to be nonlinear and seems, to some extent, to be partially synchronized chaos (as was found by Duane *et al.* (1999) for the northern and southern hemisphere blocks). For such a complex system, the only possibility for realistic modelling seems to be when only a few of the various mechanisms become prevalent in the process, so that the system dynamics are simplified with a corresponding reduction in the number of the effective degrees of freedom. Therefore, the notion of chaos theory, i.e. that seemingly complex behaviour could be the result of simple determinism influenced by only a few nonlinear interdependent variables, and the related methods of nonlinear dynamics (e.g. nonlinear prediction) could contribute to an understanding of the dynamics of interaction between particular teleconnection patterns.

One of the conceptual approaches used in chaos theory is the defining of the correlation dimension for the time series: a low dimension determines the minimal number for the degrees of freedom and, consequently, validates the applicability of the method of nonlinear prediction. Such a method is successfully used in hydrology for the modelling of annual runoff (see e.g. Sivakumar 2001). However, Kawamura *et al.* (1998) showed that low correlation dimensions are unfortunately absent in the Southern Oscillation (SO) index time series. The plausible reason is that the length of such a time series is still too short. Nevertheless, the Southern Oscillation Index (SOI) time series is characterized by a fractal power law (Ausloos and Ivanova 2001).

One of the disadvantages of chaos analysis is that the assumptions underlying it (deterministic time series without observational noise) are not realistic for the oscillation index data. Thus we analyse the monthly time series of some of the aforementioned oscillations (SO, AO, and AAO) by means of mutual information (Paluš 1995), which does not require those assumptions and has been successfully applied to time series from very different origins, such as meteorology and physiology (Paluš 1996; Diks and Mudelsee 2000). We also introduce an information theoretical test for the Granger causality (Granger 1969) and apply it to the data to obtain some insights into the causal nature of the dependence between different variables. Basing our work on the assumption that the oscillation phases depend on the observed global temperature trend,

we carry out the analysis for different periods of the twentieth century. Also, to examine the effect of time-scale on the nonlinear interaction between teleconnection patterns we use wavelet decomposition and carry out the analysis for several detail components. Thus the intent of this paper is to investigate the nonlinear interaction between the global teleconnection patterns at different time-scales.

The paper is organized as follows. In the next section we report some known intelligence on the mechanism of the evolution and relationship between main teleconnection patterns. Also, characteristic time-scales for the variability and response are described. In section 3 the data and methodology are presented; the concepts of mutual information, Granger causality and wavelet decomposition are introduced. In section 4 the main findings are discussed. Section 5 summarizes and concludes this paper.

2. Main global teleconnection patterns: some preliminaries

The aim of this section is not to describe the whole variety of mechanisms for interaction and feedbacks (for this, we recommend the following reviews: Marshall *et al.* 2001; Wanner *et al.* 2001; Turner 2004) acting between the teleconnection patterns we have selected for the analysis. Rather, the purpose is to show that (a) the indices of the AO, the ENSO, and the AAO reflect, to some extent, the atmosphere–surface interaction, and (b) our choice of the mentioned oscillations is valid for the subsequent analysis.

(*a*) *Arctic Oscillation*

The term 'Arctic Oscillation' has been introduced (Thompson and Wallace 1998) to describe the main component of sea-level pressure (SLP) variability over the northern hemisphere that has the leading mode of circulation variability with a deep, barotropic, zonally symmetric structure, a primary centre of action over the Arctic and opposing anomalies in midlatitudes. While the AO is defined as the monthly-mean, extratropical, tropospheric pattern of variability, its influence extends well beyond these categories. It has connections to extreme weather events and long-term climate trends, a distinctive signature in the tropics, and important connections to the stratosphere.

The high index of the AO (warm phase) is defined as periods of below normal Arctic SLP, enhanced surface westerlies over the North Atlantic, and warmer and wetter than normal conditions in northern Europe. During the low index of the AO (cool phase) the weather conditions are opposite.

The Arctic Oscillation is frequently compared to the NAO and PNA. Ambaum *et al.* (2001) compared the definition and interpretation of the AO and NAO. They showed that the NAO reflects the correlations between the surface pressure variability at its centres of action, whereas this is not the case for the AO. The NAO pattern can be identified in a physically consistent way in principal component analysis applied to various fields in the Euro-Atlantic region. A similar identification is found in the Pacific region for the PNA pattern, but no such identification is found here for the AO. Their results suggest that the NAO paradigm may be more physically relevant and robust for northern hemisphere variability than the AO paradigm. However, this does not disqualify many of the physical mechanisms associated with annular modes from explaining the existence of the NAO.

Deser (2000) showed that the teleconnectivity between the Arctic and midlatitudes is strongest over the Atlantic sector, and that the temporal coherence between the Atlantic and Pacific midlatitudes is weak, both on intraseasonal and interannual time-scales, during the past 50 years.

By using a simple dynamical model for the basic spatial and temporal structure of the large-scale modes of intraseasonal variability and associated variations in the

zonal index, Vallis *et al.* (2004) showed that both the NAO and the AO are produced by the same mechanism, and are manifestations of the same phenomenon.

In the present study we investigate the AO as the main teleconnection pattern in northern extratropical latitudes. Based on the above paragraphs, the principal features of the NAO can be used, to some extent, with the AO. One of these features is the atmosphere–ocean interaction in the North Atlantic sector. However, the forcing by the ocean of year-to-year changes in the NAO is a weak influence in comparison with atmospheric internal variability. The NAO is thus very different in character to the SO, and its predictability—at least on seasonal-to-interannual time-scales—is almost certainly much lower. It can also be noted that the SST anomalies tripole exerts an influence on the generation of the 7.7-year variability of the NAO (da Costa and de Verdiere 2002). Similar periodicity was found by Khokhlov *et al.* (2004) for the influence of the NAO and SO on the eddy kinetic energy content in the atmosphere of the northern tropics and midlatitudes.

The Arctic Oscillation itself (and together with the NAO) affects significantly the long-term variations of climate in the northern hemisphere. During the past decades, there has been a positive trend in the NAO (Hurrell 1995), explaining partly why climate change in the Arctic was probably faster than anywhere else in the world. Part of the observed Arctic warming may have been due to enhanced transport of anthropogenic pollution into the Arctic during the past decades, because of both increasing emissions and the positive NAO trend.

(*b*) *El Niño–Southern Oscillation*

The El Niño–Southern Oscillation is the largest climatic cycle on decadal and sub-decadal time-scales and it has a profound effect on not only the weather and oceanic conditions across the tropical Pacific, where the ENSO has its origin, but also in regions far removed from the Pacific basin. The ENSO has a very direct influence on weather conditions in some latitude areas, and its effects, for example, have been linked to the anomalies of global precipitation (Dai and Wigley 2000).

The evolution of the ENSO cycle can be measured by a number of different indices. In the present paper, we use the Southern Oscillation index, which is the normalized difference in the surface pressure between Tahiti and Darwin (Australia).

As well as for the AO/NAO case, the atmosphere–ocean interaction is realized in the ENSO. For example, by using the wavelet transform, Lucero and Rodríguez (2000) studied the decadal and interdecadal fluctuations in the equatorial Pacific SST and in the SOI. They particularly showed that there is a large correlation between the positive (negative) extreme of SOI fluctuations and associated negative (positive) extreme of SST anomaly fluctuations at decadal, bidecadal, and interdecadal time-scales. The controlling process on the variability of the decadal components of winter SOI and winter SST anomaly in 1896–1985 is a joint amplitude modulation. This amplitude modulation attains maximum amplitude in 1913–1917. Thereafter, amplitude decreases until about 1959. In the early 1960s, the amplitude modulation for the decadal fluctuations starts to grow again.

The ENSO has undergone considerable interdecadal changes over the last 125 years. By using the wavelet decomposition, Torrence and Webster (1999) showed that wavelet power spectra and variance time series display interdecadal changes in 2–7-yr variance, and give intervals of high variance (1875–1920 and 1960–90) and an interval of low variance (1920–60). Also, the 2–7-yr variance time series contain a 12–20-yr oscillation, consisting of a 12–20-yr modulation of ENSO amplitude. Also, similar periodicities

determined by the joint influence of the AO and the ENSO were found by Jevrejeva *et al.* (2003) for the highest variability in ice conditions in the Baltic Sea.

As was noted above, the ENSO affects the processes of both hemispheres. Analysing the set of multidecadal runs with the global circulation model, Hannachi (2001) showed that the familiar PNA pattern emerges as the second mode of internal variability while the first mode is reminiscent of the North Pacific Oscillation over the North Pacific. For the ensemble mean, the same PNA mode appears as the first mode of variability over the North Pacific while over the North Atlantic the first modes of variability are not too different from the corresponding modes of the internal noise. Gaussian analysis applied to the North Pacific sector indicates the PNA pattern is a synchronized response to ENSO with +PNA during El Niño and −PNA during La Niña, the amplitude of the response being proportional to the amplitude of the east tropical Pacific SST anomaly (Hannachi 2001). Moreover, the PNA behaves as a (quasi-linearly) locked mode to the ENSO while over the North Atlantic the atmospheric response is more likely nonlinear.

The inter-event variability of the atmospheric relationship between the ENSO and the North Atlantic sector could be influenced by a myriad of factors. It seems that the strength of warm and cold ENSO events is not the dominant factor. Firstly, the strongest cold and warm ENSO events are not systematically grouped into the most typical cluster. Secondly, the most consistent SLP anomaly pattern during the warm ENSO events is mainly observed between 1930 and 1970, i.e. when these events are rather weak. Nevertheless, the least homogeneous cluster for the warm ENSO events is associated with the lowest SST anomaly in Niño3 (Gouirand and Moron 2003).

Corresponding to the El Niño events, the global atmospheric circulation is modified through the changes of the Walker–Hadley circulation (Klein *et al.* 1999). This, in turn, modifies the heat flux exchanges at the air–sea interface. The SSTs of remote oceans are thus affected. Such effects were detected both for the Atlantic (Wang 2005) and for the Southern Ocean (Li 2000).

(*c*) *Antarctic Oscillation*

Although as early as in the first quarter of the twentieth century Sir Gilbert Walker had stated that: 'Just as in the North Atlantic there is a pressure opposition between the Azores and Iceland, . . . , there is an opposition between the high pressure belt across Chile and the Argentine on the one hand, and the low pressure area of Weddell Sea and the Bellingshausen Sea on the other.', the scarcity of data in the southern hemisphere hindered the search for new oscillations. During the last two decades, as more comprehensive data over the southern hemisphere became available, a new atmospheric oscillation in the middle and high southern latitudes was found, and named the Antarctic Oscillation. This term refers to a large-scale alternation of atmospheric mass between the mid- and high-latitudes.

The AAO is, *per se*, the counterpart of the AO, and emerges as the leading empirical orthogonal function of mean SLP over the southern hemisphere with associated regression patterns of temperature, zonal wind and geopotential height from the surface to the stratosphere.

(*d*) *Forced climate change and teleconnection patterns*

Many studies have shown evidence of a major climate change in the late 1970s and early 1980s. The change comprises a reversal of the sea surface temperature anomaly pattern in the North Pacific Ocean, a lowering of the atmospheric geopotential height in

the North Pacific, altered frequency and intensity of cyclones/anticyclones and severe storms in mid- and high latitudes, along with an 'abrupt' increase of the northern hemisphere (NH) average surface air temperature. It is natural that these changes affect the teleconnection patterns.

Hu *et al.* (2004) showed that in 1979–2000 significant increases of the NH summer and winter season kinetic energy, both mean and eddy, were observed in comparison with 1948–78. The increase has resulted from increased conversion rates from the mean to the eddy available potential energy and then from the eddy available potential energy to the eddy and mean kinetic energy. Keeping in mind that the eddy kinetic energy is well correlated with the NAO and ENSO at the long time-scale (Khokhlov *et al.* 2004), one can suppose that the observed warming effects significant changes in the teleconnection patterns.

Moreover, some simulations with numerical models indicate that a response to the greenhouse forcing is found both for the ENSO and for the annular modes (AO and AAO). For example, Cai and Whetton (2000) reported results from experiments using the CSIRO (Commonwealth Scientific and Industrial Research Organization) Mark 2 CGCM (Climate General Circulation Model) which show a warming pattern that is initially La Niña-like, but after the 1960s El Niño-like. Their results show that a linkage between tropical and extratropical ocean circulation can cause an initial warming pattern to change. Also, climate change simulations for 1900–2100, with forcing due to greenhouse gases and aerosols, exhibit positive trends in both the AO and the AAO (Fyfe *et al.* 1999). Their results do not suggest that a simulated trend in the AO/AAO necessarily depends on stratospheric involvement nor that forced climate change will be expressed as a change in the occurrence of one phase of the AO/AAO over another. This pattern of climate change projects exclusively on the AAO pattern in the southern hemisphere but not in the NH.

Thus, there is ample evidence that most of the atmospheric circulation variability in the form of the North Atlantic Oscillation (NAO) arises from the internal, nonlinear dynamics of the extratropical atmosphere (see e.g. Thompson *et al.* 2003). From our point of view, such nonlinear dynamics is the characteristic feature for the whole global atmosphere.

3. Data and methodology

(*a*) *Data*

We use unsmoothed datasets for the indices of the AO, the SO, and the AAO, as well as for the global temperature anomaly (T) from the base period 1961–90. All data were obtained via the Internet (http://www.jisao.washington.edu/data_sets/aots/ao18992002, http://www.cru.uea.ac.uk/ftpdata/soi.dat, http://www.jisao.washington.edu/data/aao/slp/aaoslppc19482002, http://www.cru.uea.ac.uk/ftpdata/tavegl2v.dat respectively). Figure 1 shows the time series chosen for the analysis. The Arctic Oscillation Index (AOI) and the Antarctic Oscillation Index (AAOI) were calculated from the SLP anomalies north of 20°N and south of 20°S, respectively (Thompson and Wallace 1998, 2000). The SOI was defined as the normalized pressure difference between Tahiti and Darwin using the method given by Ropelewski and Jones (1987). The global average temperature anomaly was calculated using over 3000 monthly station temperature time series over land regions and sea surface temperature measurements taken on board merchant and some naval vessels. To avoid biases that could result from the problems concerned with measurements, monthly average temperatures are reduced to anomalies from the period with best coverage (1961–90). Further details of this data set are

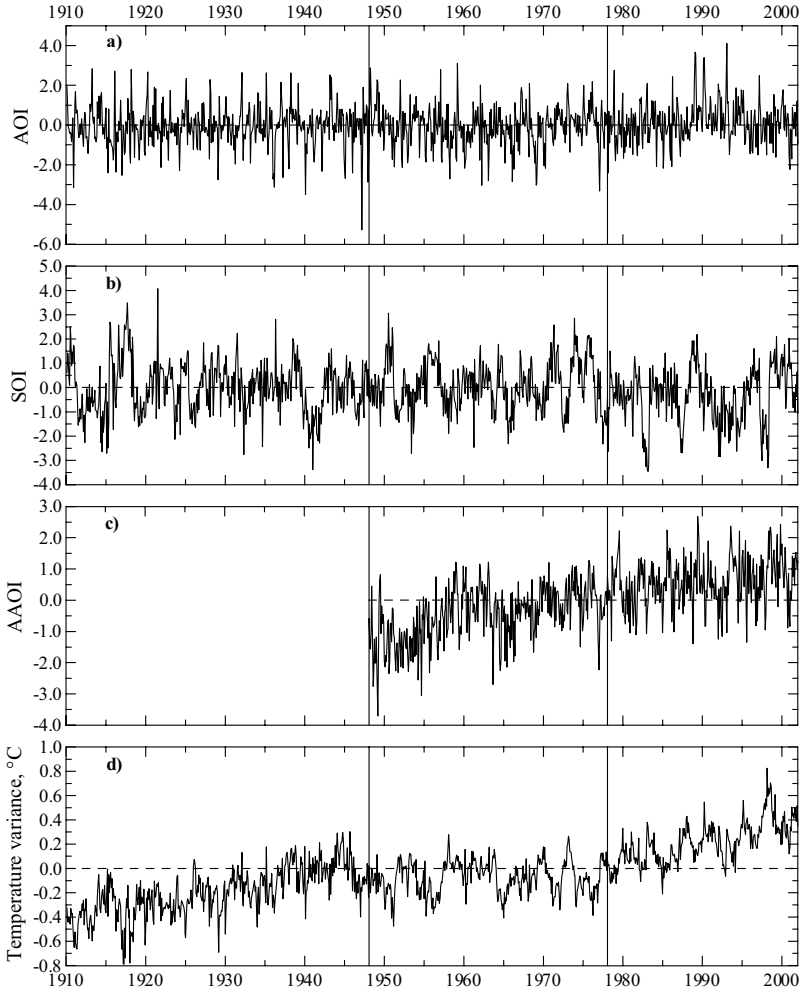

Figure 1. Original time series of (a) the Arctic Oscillation index, (b) the Southern Oscillation index, (c) the Antarctic Oscillation index, and (d) the global temperature anomaly during 1910–2001. The x-axis is the calendar year.

given for land regions by Jones and Moberg (2003) and for the oceans by Rayner *et al.* (2003). From the original datasets, we extract time series from 1910 until 2001 (except for the AAOI that starts from 1948). For further analysis, we divide the time series into three epochs: 1910–47, 1948–77 and 1978–2001 (hereafter W1, C and W2 respectively). The first and third epochs are characterized by global warming while during the second epoch the reverse process is observed. The first reason for dividing the time series into three epochs (we use this term conditionally) is the assumption that the relationship between main teleconnection patterns varies in the periods of relative warming or cooling. Furthermore, it was supposed that this relationship itself can cause the temperature variations. From our point of view, roughly comparable cross-redundancies and Granger causalities for the two epochs of warming and radically different ones for the epoch of cooling can be considered as confirmation of this linkage. Another reason lies in the different quality of the original time series used for calculating the indices and temperature during the twentieth century. From this point of view, the last epoch is the most

representative sample. The periods of warming and cooling are displayed comparatively well in Fig. 1(d), though these trends of temperature are shown more fully by Folland *et al.* (2001).

(*b*) *Mutual information and cross-redundancy*

Consider two discrete variables X and Y with joint probability density functions (PDF) $f_{X,Y}(x, y)$, and marginal PDF $f_X(x)$ and $f_Y(y)$ respectively. The mutual information $I(X, Y)$ quantifies the average amount of common information contained in the variables X and Y:

$$I(X, Y) = \iint f_{X,Y}(x, y) \log \frac{f_{X,Y}(x, y)}{f_X(x) f_Y(y)} \, \mathrm{d}x \, \mathrm{d}y. \tag{1}$$

The mutual information can be considered as a nonlinear analogue of the correlation between X and Y. The mutual information is symmetric, non-negative and equal to zero if and only if X and Y are independent.

Prichard and Theiler (1995) proposed the generalization of mutual information, by expressing it in terms of generalized correlation integrals $C_q(\epsilon)$. In particular, they gave:

$$I_q(X, Y; \epsilon) = \log C_q(X, Y; \epsilon) - \log C_q(X; \epsilon) - \log C_q(Y; \epsilon). \tag{2}$$

This form enables convenient estimation by means of plug-in estimates of C_q. The choice $q = 2$, the value which will be used throughout this paper, is particularly convenient since the estimation of the correlation integral for this case is straightforward. To estimate the correlation integrals, we use the algorithm proposed by Grassberger and Procaccia (1983), which uses the reconstruction of the phase-space. For the scale parameter we chose $\epsilon = 0.5$.

To compare later on the results obtained by nonlinear method with those determined by linear technique, we use the linearized version of mutual information based on the method introduced by Prichard and Theiler (1995):

$$\lambda(X, Y) = -\tfrac{1}{2} \log\{1 - (L_{X,Y})^2\}, \tag{3}$$

where $L_{X,Y} = \langle XY \rangle^{1/2}$ is the cross-correlation function between X and Y, which can be calculated as Pearson's correlations. Using Eq. (3) assumed that both variables have zero mean and unit variance.

Furthermore, to examine the relation between two variables in more detail, we determine the mutual information and its linearized version of the time series as a function of the delay (termed cross-redundancy and linearized cross-redundancy in Prichard and Theiler (1995)).

The estimation of mutual information requires the calculation of the correlation integral. Since we divide the twentieth century into three epochs as was mentioned in section 3(a), the lengths of separate time series are comparatively small. At the same time, the lengths of the original samples for the SOI, AO and AAOI are equal to 1860, 1248 and 660, respectively. We calculated the correlation integrals for both the original series and the separate epochs. Our estimates show that these correlation integrals are almost equal for all cases, i.e. the reconstruction of phase space is realized with the same level of accuracy independently of length of sample. Therefore we assume that the sample length of separate epochs is enough to trust the results obtained in this study.

(*c*) *Granger causality*

Using the cross-redundancy, we only examine the dependence between two variables, but do not obtain a behaviour of coupling. For example, if there is nonlinear

dependency between two variables, this might be because the first variable is driving the second, or the second is driving the first, or both these events (feedback). Such a causal relationship can be examined by testing for the Granger causality (Granger 1969).

This well-known concept used in econometrics is based on predictability. According to Granger (1969), the following sentence can be stated. Y is a Granger cause of X if past values of Y can improve predictions of future values of X, conditionally on past values X and Y, which are distributed differently than future values based on X only. In this case X is conditionally (on past values of X) dependent on Y. This definition of causality is only operational and leaves open the possibility that causality is found between X and Y when they are in fact uncoupled. This can be the case if both X and Y are driven by a third variable (Diks and Mudelsee 2000).

The definitions can clearly be generalized to be operative for a specified time. One could then talk of causality existing at this moment of time. The one completely unreal aspect of the above definitions is the use of series representing all available information.

Granger causality was formulated for linear models, and its application to nonlinear systems may or may not be appropriate, depending on the specific problem. We previously used the method proposed by Chen *et al.* (2004) to estimate extended Granger causality, which can be applied to nonlinear time series, particularly those shown in Fig. 1(c) and 1(d), together with ordinary Granger causality. As a result of this application, nonlinear and linear causality were found to be very similar. We leave out the results using the nonlinear version in this paper.

Let us illustrate the above definition using a model with two variables.

Let X_t, Y_t be two stationary time series with zero means. The simple causal model is

$$\left.\begin{aligned} X_t &= \sum_{j=1}^{m} a_j X_{t-j} + \sum_{j=1}^{m} b_j Y_{t-j} + \nu_t, \\ Y_t &= \sum_{j=1}^{m} c_j X_{t-j} + \sum_{j=1}^{m} d_j Y_{t-j} + \eta_t, \end{aligned}\right\} \tag{4}$$

where ν_t, η_t are taken to be two uncorrelated white-noise series. In Eq. (4) m can equal infinity but in practice, of course, due to the finite length of available data, m is assumed finite and shorter than the given time series.

The definition of causality given above implies that Y_t is causing X_t provided some b_j is not zero. Similarly, X_t is causing Y_t if some c_j is not zero. If both of these events occur, there is said to be a feedback relationship between X_t and Y_t.

Since Eq. (4) is the vector autoregressive model, then we use standard techniques to estimate the model (e.g. methods described by Lütkepohl (1991)). The probability of Granger causality is the solution of the model.

(*d*) *Non-decimated wavelet transform*

Wavelets are fundamental building block functions, analogous to the trigonometric sine and cosine functions. A Fourier transform extracts details from the signal frequency, but all information about the location of a particular frequency within the signal is lost. In comparison, the multi-resolution analysis makes wavelets particularly appealing for this study, because they are localized in time and the signals are examined using widely varying levels of focus. For details about wavelet theory, the monographs of Daubechies (1992) and Goswami and Chan (1999) can be recommended. In this article, we work with non-decimated (discrete) wavelet transform rather than continuous wavelet transform, because from a statistical point of view, they are well adapted

(i.e. to the search for correlations or noise reduction) and offer a very flexible tool for analysis of discrete time series such as the ones under study here. The advantages of non-decimated wavelet transform also include (1) a much better temporal resolution at coarser scales than with ordinary discrete wavelet transform, and (2) the fact that it allows us to isolate time series of the major components of meteorological signals in a direct way.

The dilation and translation of one mother wavelet $\psi(t)$ generates the wavelet $\psi_{j,k}(t) = 2^{j/2}\psi(2^j t - k)$, where $j, k \in \mathbf{Z}$ (the set of all integers). The dilation parameter j controls how large the wavelet is, and the translation parameter k controls how the wavelet is shifted along the t-axis. For a suitably chosen mother wavelet $\psi(t)$, the set $\{\psi_{j,k}\}_{j,k}$ provides an orthogonal basis, and the function f which is defined on the whole real line can be expanded as

$$f(t) = \sum_{k=-\infty}^{\infty} c_{0k}\varphi_{0,k}(t) + \sum_{j=1}^{J}\sum_{k=-\infty}^{\infty} d_{jk}\psi_{j,k}(t) \tag{5}$$

where $\varphi(t)$ is the scaling function, the maximum scale J is determined by the number of data, the coefficients c_{0k} represent the lowest frequency smooth components, and the coefficients d_{jk} deliver information about the behaviour of the function f concentrating on effects of scale around 2^{-j} near time $k \times 2^{-j}$. This wavelet expansion of a function is closely related to the discrete wavelet transform (DWT) of a signal observed at discrete points in time.

In practice, the length of the signal, say n, is finite and, for our study, the data are available monthly, i.e. the function $f(t)$ in Eq. (5) is now a vector $\mathbf{f} = (f(t_1), \ldots, f(t_n))$ with $t_i = i/n$ and $i = 1, \ldots, n$. With these notations, the DWT of a vector $\mathbf{f}$ is simply a matrix product $\mathbf{d} = \mathbf{W}\mathbf{f}$, where $\mathbf{d}$ is an $n \times 1$ vector of discrete wavelet coefficients indexed by two integers, d_{jk}, and $\mathbf{W}$ is an orthogonal $n \times n$ matrix associated with the wavelet basis. For computational reasons, it is simpler to perform the wavelet transform on time series of dyadic (power of 2) length.

One particular problem with DWT is that it is not translation invariant. This can lead to Gibbs-type phenomena and other artefacts in the reconstruction of a function. The non-decimated wavelet transform (NWT) of the data $(f(t_1), \ldots, f(t_n))$ at equally spaced points $t_i = i/n$ is defined as the set of all DWTs formed from the n possible shifts of the data by amounts i/n; $i = 1, \ldots, n$. Thus, unlike the DWT, there are 2^j coefficients on the jth resolution level, and there are n equally spaced wavelet coefficients in the NWT: $d_{jk} = n^{-1}\sum_{i-1}^{n} 2^{j/2}\psi\{2^j(i/n - k/n)\}y_i$, $k = 0, \ldots, n-1$ on each resolution level j. This results in $\log_2(n)$ coefficients at each location. As an immediate consequence, the NWT becomes translation invariant. Due to its structure, the NWT implies a finer sampling rate at all levels and thus provides a better exploratory tool for analysing changes in the scale (frequency) behaviour of the underlying signal in time. These advantages of the NWT over the DWT in time series analysis are demonstrated in Nason *et al.* (2000).

From the above paragraphs, it is easy to map any time series into the wavelet domain. Another way of viewing the result of an NWT is to represent the temporal evolution of the data at a given scale. This type of representation is very useful to compare the temporal variation between different time series at a given scale. To obtain such results, the smooth signal S_0 and the detail signals D_j $(j = 1, \ldots, J)$ are defined as follows:

$$S_0(t) = \sum_{k=-\infty}^{\infty} c_{0k}\varphi_{0,k}(t) \quad \text{and} \quad D_j(t) = \sum_{k=-\infty}^{\infty} d_{jk}\psi_{0,k}(t). \tag{6}$$

Sequentially, the temporal multi-resolution decomposition of a signal is derived from

$$D_j(t) = S_j(t) - S_{j-1}(t).$$

The fine-scale features (high frequency oscillations) are captured mainly by the fine-scale detail components D_J and D_{J-1}. The coarse-scale components S_0, D_1, and D_2 correspond to lower frequency oscillations of the signal. Note that each band is equivalent to a band-pass filter.

Further, we use the Daubechies wavelet (db15) as mother wavelet. This wavelet is biorthogonal, supports discrete wavelet transform and has no explicit expression (Daubechies 1992). The choice of mother wavelet was realized by the estimation of Shannon entropy (Coifman and Wickerhauser 1992) reaching its minimum for different decompositions.

In this paper we consider periods with a non-dyadic number of months. Therefore, whole periods are divided into two sub-periods with dyadic length of months. Then the NWT is applied to these sub-periods and derived detail components are 'glued' together to obtain the maximum possible length.

4. Cross-redundancies and Granger causality for unsmoothed time series

Figure 2 shows the cross-redundancy and Granger causality for unsmoothed, unfiltered time series of oscillations and the global average temperature anomaly. Before analysing, let us note some particularities concerning the interpretation of results represented on the graphs. For a particular graph, the heading notation reveals: (i) values for which results are presented; (ii) the lagged value; and (iii) the epoch under consideration. For example, 'AOI-T (W1)' in Fig. 2(a) denotes the cross-redundancies for the lagged AOI and T during the W1 epoch. Also, only positive values for the cross-redundancies indicate that there is a relationship between variables. In these graphs, the magnitudes for the possibility of Granger causality are denoted as triangles. If these values are located in the area of positive lags, then, e.g. for Fig. 2(a), the AOI is the Granger cause of the T and vice versa. Note that throughout this paper the Granger causality is estimated at 95% significance level.

Figure 2 shows also the linearized cross-redundancies (dotted lines). In contrast to the cross-redundancy, many of the significant peaks are reduced or absent in the linearized version, suggesting that these peaks are the result of nonlinear relationships. Therefore this result can be a justification for the use of nonlinear measure rather than its linearized version.

It can be noted that Fig. 2 shows many features of the interaction between the teleconnection patterns, which was described in section 2. For example, the AO–SO interaction occurs, though it is weak. Moreover, during the C epoch the cross-redundancy for these oscillations tends to increase with lags, whereas during the W1 and W2 epochs the cross-redundancies are rather insignificant. Here, it is surprising that the AO is the Granger cause of SO; it is observed at almost the same lags (12–24 months) during both the W1 epoch and the C epoch.

The largest cross-redundancy is registered for the T and SOI. During the C epoch, it is almost symmetric with regard to the maximum at zero lag, whereas in the W2 epoch this maximum shifts towards positive lags (15 months approximately). Also, the temperature anomaly is the Granger cause of the SOI.

The most interesting feedbacks are registered for the Antarctic Oscillation. First, during the C epoch the SOI is the Granger cause of the AAOI with lags close to 30 months, whereas the AAOI causes the SOI with lags less than 10 months.

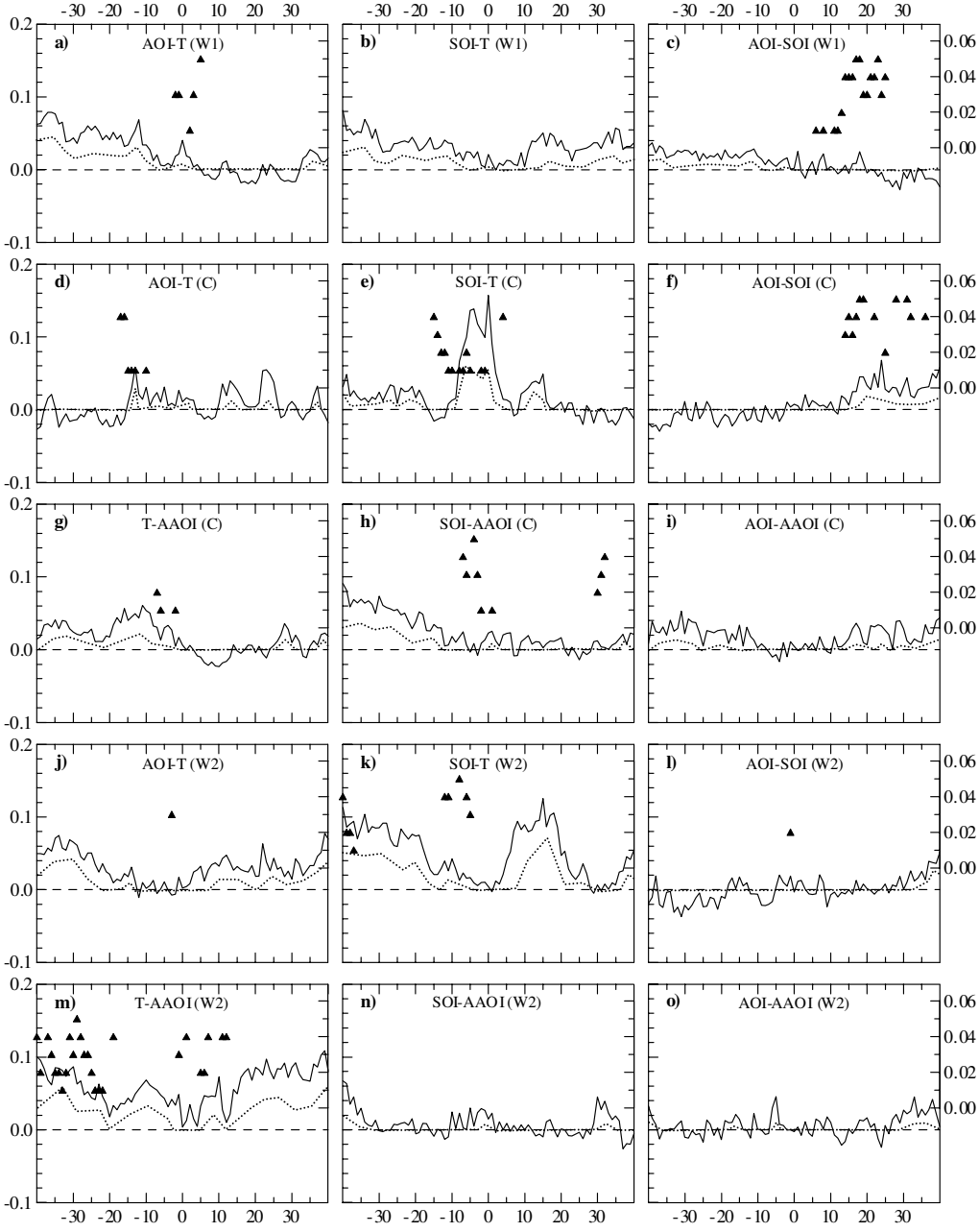

Figure 2. Cross-redundancies (solid lines; left *y*-axis), linearized cross-redundancies (dotted lines; left *y*-axis), and probabilities of Granger causality (triangles; right *y*-axis) subject to the lag (*x*-axis; month) for the different indices of oscillation and global temperature anomalies during three epochs in the twentieth century.

Second, during the W2 epoch the temperature anomalies force the AAOI with lag up to 12 months, but the AAOI itself is the Granger cause of the T with lags larger than 24 months.

In some cases, the cross-redundancies are small and the Granger causalities are insignificant at the prescribed significance level, e.g. for the relationship between the AOI and AAOI.

So, the obtained results mostly agree with experimental and observational data, though by using known feedbacks it is difficult to explain some of them, in particular, in relation to the fact that the AOI is the Granger cause of the SOI. The latter can be rather ascribed to the deficient quality of an unfiltered time series with so-called 'white noise'.

5. Cross-redundancies and Granger causality for wavelet detail components

Since wavelet decomposition is an analogue of band-pass filtering, one can assume that it provides 'pure' separate signals of various periodicities. Our preliminary findings (not presented here) show that the cross-redundancy for high-frequency detail components are barely different from those for the unfiltered time series. Starting with the 5-year periodicity variations, the cross-redundancies enlarge significantly (by 3–4 times). Therefore, in this section we consider two low-frequency detail components: D_5 with periodicity from 5 to 7 years and D_4 with more than decadal variability. Figure 3 shows these components for the analysed time series. These detail components seem more coherent (to some extent) in contrast to the unfiltered time series. Consequently, it can be expected that the nonlinear relationship in this case must be more essential.

Figure 4 shows the cross-redundancy and Granger causality for the detail components D_5. These components are attractive because the ENSO and AO possess almost the same periodicities. In this case, the nonlinear relationship between the teleconnection patterns emerges more clearly. First, the cross-redundancy for the AOI and SOI is positive almost everywhere. Also, the Granger causality shows that there is a feedback between these indices during the epochs W1 and C at lags near 18 months. Second, in contrast with the unfiltered time series, nonlinear dependence between the AOI and AAOI occurs; in the C epoch it emerges as a feedback at lags of more than 20 months. Third, feedback is registered for the relationship between the SOI and AAOI; in this case the cross-redundancy amounts to the maximum, and the difference between maxima of cross-redundancy in the epochs W1 and C is approximately 12 months.

Also, the climatic forcing of teleconnection patterns (or inverse process) appears for the detail components. For example, in the C epoch the temperature anomalies are rather the Granger cause of the AAOI, whereas during the warming epoch the reverse behaviour is observed. Furthermore, in the warming epochs the feedback between the T and AOI emerges, but it is not so evident in the case of the SOI.

Figure 5 displays the cross-redundancy and Granger causality for the detail components D_4 with a periodicity of more than 10 years. Here, the largest (in the mean) and the positive values of cross-redundancy are registered. From our point of view, the results obtained for the C epoch are highly noteworthy. The asymmetric behaviour of the interactions between the T, on the one hand, and the indices of the Arctic Oscillation and the Southern Oscillation, on the other hand, is observed (see Fig. 5(d) and (e)). In other words, when the largest nonlinear interaction between the T and AOI is registered, the minimal relationship between the T and SOI occurs, whereas the detail components of the AOI and SOI are very similar (see Fig. 3). Also, in both cases the Granger causality emerges for both maxima and minima. The cross-redundancies for the T–AAOI and

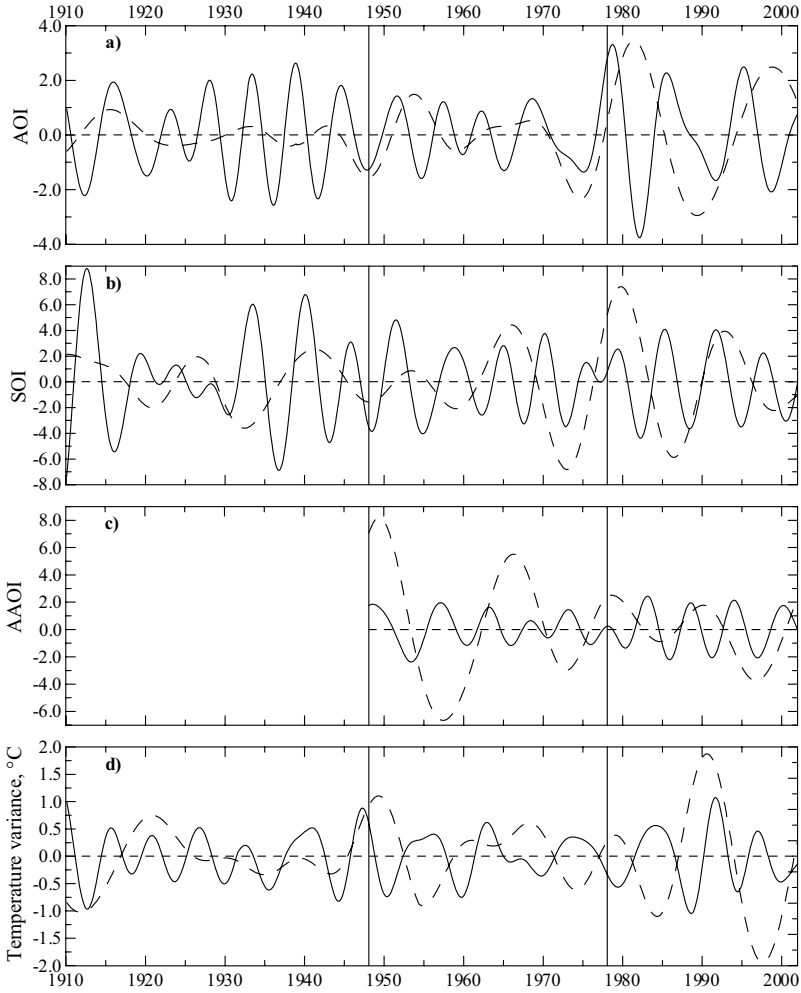

Figure 3. Wavelet detail components D_5 (solid lines) and D_4 (dashed lines) of (a) the Arctic Oscillation index, (b) the Southern Oscillation index, (c) the Antarctic Oscillation index, and (d) the global temperature anomaly during 1910–2001. The x-axis is the calendar year.

SOI–AAOI behave almost similarly, and the nonlinear relationship between the AOI and AAOI, as well as between the AOI and SOI (to a lesser degree), varies slightly.

As well as in the case of unsmoothed time series, the linearized versions of cross-redundancy are significantly smaller than the nonlinear ones.

6. Conclusions and discussion

In this study we use non-fully traditional (for meteorology) methods to examine the nonlinear interaction between some teleconnection patterns during different epochs of the twentieth century. The purpose is to reveal the chaotic behaviour in the global climate system. The main advantage of the cross-redundancy and Granger causality, in contrast to other chaotic analysis, is because of the relatively short time series used

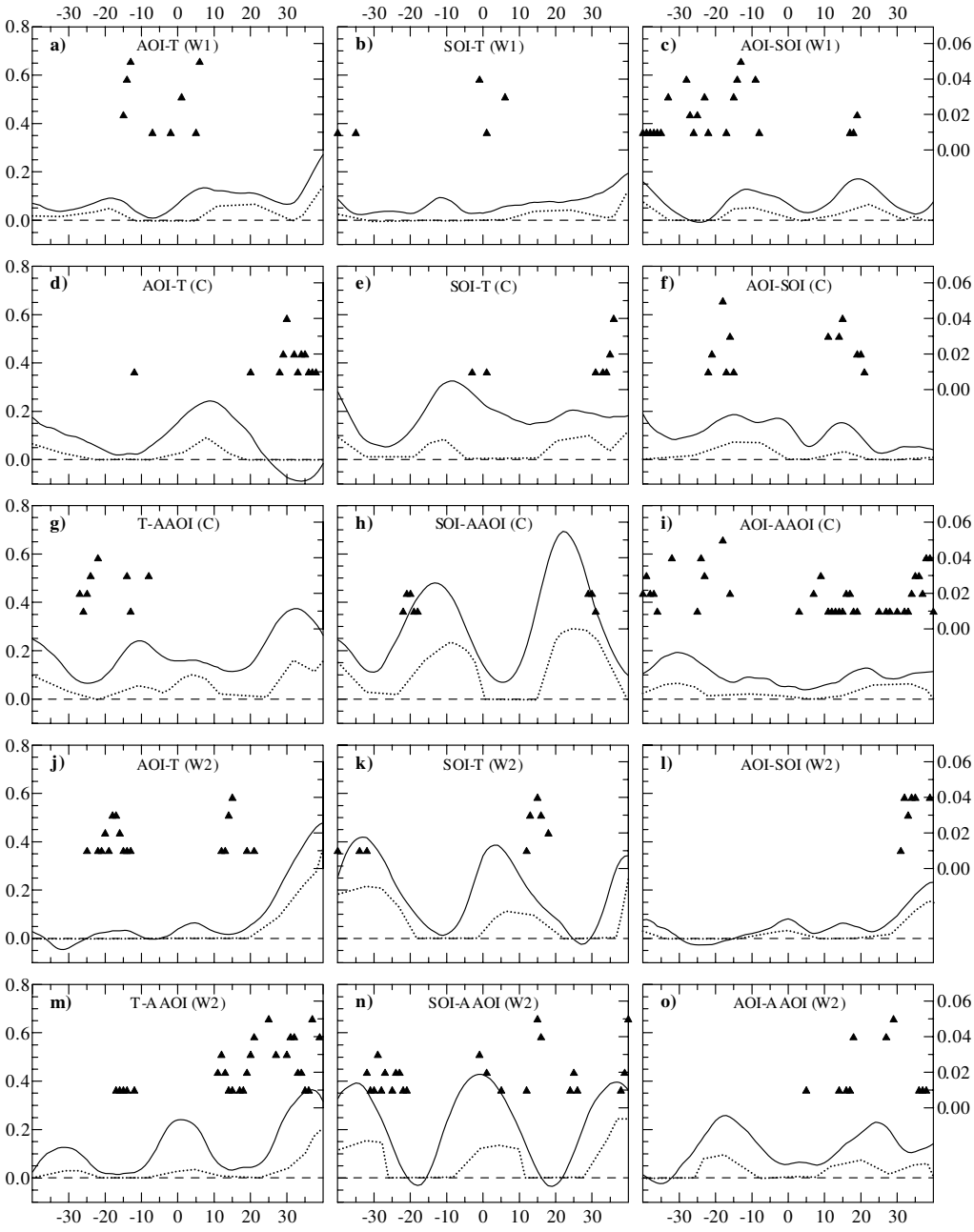

Figure 4. Cross-redundancies (solid lines; left y-axis), linearized cross-redundancies (dotted lines; left y-axis), and probabilities of Granger causality (triangles; right y-axis) subject to the lag (x-axis; month) for the wavelet detail component D_5 for the different indices of oscillation and global temperature anomalies during three epochs in the twentieth century.

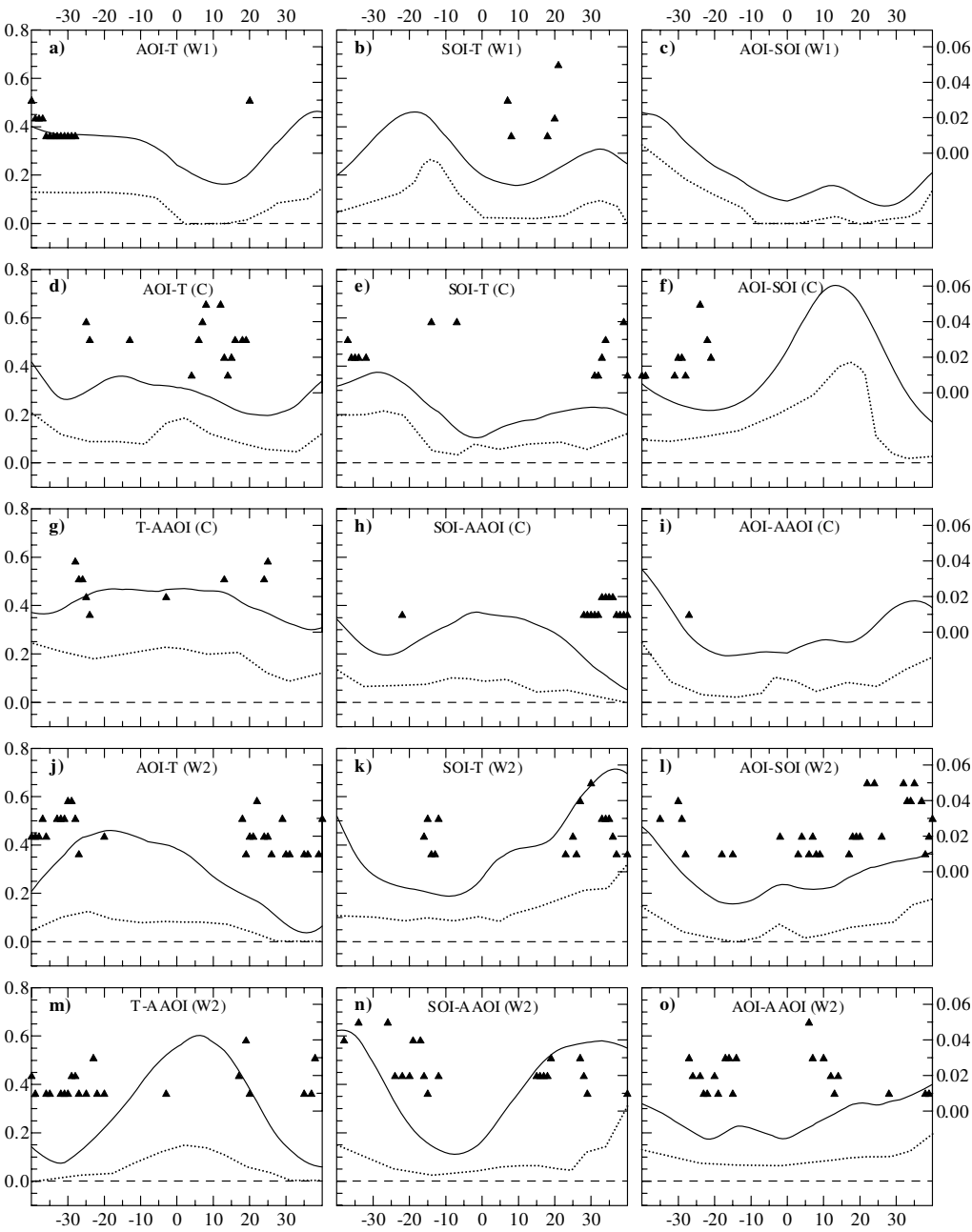

Figure 5. As Fig. 4, but for wavelet detail component D_4.

as input parameters for these approaches. Furthermore, to study the influence of low-frequency variations, wavelet decomposition is applied. By assuming that the non-decimated wavelet transform extracts the 'pure' low frequency variations, the interaction at the intra- and inter-decadal time scales is considered.

Our findings show that the aforementioned methods allow us to display well-known mechanisms and feedbacks, also that application of nonlinear cross-redundancy reveals

some relationships uncovered (or not) by the linear methods. This relates above all to the relationship between the ENSO and AAO. For the daily data during December–January–February of 1979–2000, Carvalho *et al.* (2005) showed that the Southern annular mode weakens (strengthens) during warm (cold) ENSO episodes. A similar result is obtained in our paper (but for monthly time series) for low-frequency components of the SOI, AOI and AAOI (Fig. 4(i) and (n)), as well as for the original time series (Fig. 2(i) and (n)), though in the case of AOI this relationship is weaker. Also, the alternation of annular mode phases seems to be linked to the latitudinal migration of the subtropical upper-level jet and variations in the intensity of the polar jet. On the other hand, Wittman *et al.* (2005) showed that occurrence of the annular mode is a simple consequence of the north–south migration of the jet, although their stochastic model consists of a zonal jet, which is represented by a simple function of latitude and time.

Nevertheless, some of our results require further elucidation. This is first related to the feedbacks between the Arctic Oscillation and the Antarctic Oscillation. Most likely, in this case the influence of the Southern Oscillation can be a good candidate for explaining this relation. The second surprising result consists of the fact that the Arctic Oscillation can be the Granger cause of the Southern Oscillation.

By using the results obtained in this paper, we cannot conclude that global warming (or cooling) affects the interaction between the teleconnection patterns. In most studies, the ENSO is considered as one of the main internal climate modulators. By examining the components of the climate-change response that projects onto the model pattern of ENSO variability in 20 coupled global circulation models, Collins (2005) showed that the most likely scenario (with probability equals to 0.59) is for no trend towards either mean El Niño-like or La Niña-like conditions. Thus, the variations in the relationships between the global teleconnection patterns can be caused by the nonlinearity of the ENSO cycle. For example, results of An *et al.* (2005) indicate that the nonlinearity of the ENSO cycle has become stronger since the late 1970s. Of course, the period of exhaustive observation is too short. Moreover, such a period with regard to the indices of the Antarctic Oscillation starts in the late 1970s. Therefore, we divide the period from 1910 to 2001 to avoid, as far as possible, the superposition of different epochs that can be observed if we use the whole period.

From our point of view, future investigations can be realized in two ways. First, to explain some feedbacks revealed in this paper, runs with coupled global circulation models are needed. Second, our findings can be used to create a model of global climate variations based, for example, on the concept of synchronized chaos.

Acknowledgements

We thank the authors of Worldwide Web resources mentioned in section 3(a) for the possibility of access to the datasets for the indices of teleconnection patterns. We are greatly indebted to two anonymous reviewers for careful and extensive comments on the paper which has improved the presentation.

References

Ambaum, M. H. P., Hoskins, B. J. and Stephenson, D. B. 2001 Arctic Oscillation or North Atlantic Oscillation? *J. Climate*, **14,** 3495–3507

An, S.-I., Hsieh, W. W. and Jin, F.-F. 2005 A nonlinear analysis of the ENSO cycle and its interdecadal changes. *J. Climate*, **18,** 3229–3239

Ausloos, M. and Ivanova, K. 2001 Power-law correlations in the southern-oscillation-index fluctuations characterizing El Niño. *Phys. Rev. E*, **63,** 047201

Cai, W. and Whetton, P. H. 2000 Evidence for a time-varying pattern of greenhouse warming in the Pacific Ocean. *Geophys. Res. Lett.*, **27,** 2577–2580

Carvalho, L. M. V., Jones, C. and Ambrizzi, T. 2005 Opposite phases of the Antarctic Oscillation and relationships with intraseasonal to interannual activity in the tropics during the austral summer. *J. Climate*, **18,** 702–718

Chen, Y., Rangarajan, G., Feng, J. and Ding, M. 2004 Analyzing multiple nonlinear time series with extended Granger causality. *Phys. Lett. A*, **324,** 26–35

Coifman, R. R. and Wickerhauser, M. V. 1992 Entropy-based algorithms for best basis selection. *IEEE Trans. Information Theory*, **38,** 713–718

Collins, M. 2005 El Niño- or La Niña-like climate change? *Clim. Dyn.*, **24,** 89–104

da Costa, E. D. and de Verdiere, A. C. 2002 The 7.7-year North Atlantic Oscillation. *Q. J. R. Meteorol. Soc.*, **128,** 797–817

Dai, A. and Wigley, T. M. L. 2000 Global patterns of ENSO-induced precipitation. *Geophys. Res. Lett.*, **27,** 1283–1286

Daubechies, I. 1992 *Ten lectures on wavelets.* SIAM, Philadelphia

Deser, C. 2000 On the teleconnectivity of the 'Arctic Oscillation'. *Geophys. Res. Lett.*, **27,** 779–782

Diks, C. and Mudelsee, M. 2000 Redundancies in the Earth's climatological time series. *Phys. Lett. A*, **275,** 407–414

Duane, G. S., Webster, P. J. and Weiss, J. B. 1999 Co-occurrence of northern and southern hemisphere blocks as partially synchronized chaos. *J. Atmos. Sci.*, **56,** 4183–4205

Folland, C. K., Karl, T. R., Christy, J. R., Clarke, R. A., Gruza, G. V., Jouzel, J., Mann, M. E., Oerlemans, J., Salinger, M. J. and Wang, S.-W. 2001 'Observed climate variability and change'. Pp. 99–181 in *Climate Change 2001: The Scientific Basis. Contribution of Working Group I to the Third Assessment Report of the Intergovernmental Panel on Climate Change*. Eds. J. T. Houghton, Y. Ding, D. J. Griggs, M. Noguer, P. J. van der Linden, X. Dai, K. Maskell and C. A. Johnson. Cambridge University Press, Cambridge

Fyfe, J. C., Boer, G. J. and Flato, G. M. 1999 The arctic and antarctic oscillations and their projected changes under global warming. *Geophys. Res. Lett.*, **26,** 1601–1604

Gong, D. and Wang, S. 1999 Definition of Antarctic oscillation index. *Geophys. Res. Lett.*, **26,** 459–462

Goswami, J. C. and Chan, A. K. 1999 *Fundamentals of wavelets: theory, algorithms, and applications*. Wiley, New York

Gouirand, I. and Moron, V. 2003 Variability of the impact of El Niño–Southern Oscillation on sea-level pressure anomalies over the North Atlantic in January to March (1874–1996). *Int. J. Climatol.*, **23,** 1549–1566

Granger, C. W. J. 1969 Investigating causal relations by econometric models and cross-spectral methods. *Econometrica*, **37,** 424–438

Grassberger, P. and Procaccia, I. 1983 Measuring the strangeness of strange attractors. *Physica D*, **9,** 189–208

Hannachi, A. 2001 Toward a nonlinear identification of the atmospheric response to ENSO. *J. Climate*, **14,** 2138–2149

Hu, Q., Tawaye, Y. and Feng, S. 2004 Variations of the northern hemisphere atmospheric energetics: 1948–2000. *J. Climate*, **17,** 1975–1986

Hurrell, J. W. 1995 Decadal trends in the North Atlantic Oscillation: Regional temperatures and precipitation. *Science*, **269,** 676–679

Hurrell, J. W., Hoerling, M. P., Phillips, A. S. and Xu, T. 2004 Twentieth century North Atlantic climate change. Part I: assessing determinism. *Clim. Dyn.*, **23,** 371–390

Jevrejeva, S., Moore, J. C. and Grinsted, A. 2003 Influence of the Arctic Oscillation and El Niño–Southern Oscillation (ENSO) on ice conditions in the Baltic Sea: The wavelet approach. *J. Geophys. Res.*, **108,** 4677, doi: 10.1029/2003JD003417

Jones, P. D. and Moberg, A. 2003 Hemispheric and large-scale surface air temperature variations: An extensive revision and an update to 2001. *J. Climate*, **16,** 206–223

Kawamura, A., McKerchar, A. I., Spigel, R. H. and Jinno, K. 1998 Chaotic characteristics of the Southern Oscillation Index time series. *J. Hydrol.*, **204,** 168–181

Khokhlov, V. N., Glushkov, A. V. and Tsenenko, I. A. 2004 Atmospheric teleconnection patterns and eddy kinetic energy content: wavelet analysis. *Nonlinear Processes in Geophys.*, **11,** 295–301

Klein, S. A., Soden, B. J. and Lau, N.-C. 1999 Remote sea surface temperature variations during ENSO: Evidence for a tropical atmosphere bridge. *J. Climate*, **12,** 917–932

Li, Z. X. 2000 Influence of Tropical Pacific El Niño on the SST of the Southern Ocean through atmospheric bridge. *Geophys. Res. Lett.*, **27,** 3505–3508

Lorenz, E. N. 1963 Deterministic nonperiodic flow. *J. Atmos. Sci.*, **20,** 130–141
1970 Climate change as a mathematical problem. *J. Appl. Meteorol.*, **9,** 325–329

Lucero, O. A. and Rodríguez, N. C. 2000 Statistical characteristics of interdecadal fluctuations in the Southern Oscillation and the surface temperature of the equatorial Pacific. *Atmos. Res.*, **54,** 87–104

Lütkepohl, H. 1991 *Introduction to multiple time series analysis.* Springer-Verlag, New York

Marshall, J., Kushnir, Y., Battisti, D., Chang, P., Czaja, A., Dickson, R., Hurrell, J., McCartney, M., Saravanan, R. and Visbeck, M. 2001 North Atlantic climate variability: phenomena, impacts and mechanisms. *Int. J. Climatol.*, **21,** 1863–1898

Monahan, A. H., Fyfe, J. C. and Flato, G. M. 2000 A regime view of northern hemisphere atmospheric variability and change under global warming. *Geophys. Res. Lett.*, **27,** 1139–1142

Nason, G., von Sachs, R. and Kroisandt, G. 2000 Wavelet processes and adaptive estimation of the evolutionary wavelet spectrum. *J. R. Stat. Soc. B*, **62,** 271–292

Oh, H.-S., Ammann, C. M., Naveau, P., Nychka, D. and Otto-Bliesner, B. L. 2003 Multi-resolution time series analysis applied to solar irradiance and climate reconstructions. *J. Atmos. Solar-Terr. Phys.*, **65,** 191–201

Paluš, M. 1995 Testing for nonlinearity using redundancies: Quantitative and qualitative aspects. *Physica D*, **80,** 186–205
1996 Detecting nonlinearity in multivariate time series. *Phys. Lett. A*, **213,** 138–147

Prichard, D. and Theiler, J. 1995 Generalized redundancies for time series analysis. *Physica D*, **84,** 476–493

Rayner, N. A., Parker, D. E., Horton, E. B., Folland, C. K., Alexander, L. V, Rowell, D. P., Kent, E. C. and Kaplan, A. 2003 Global analyses of sea surface temperature, sea ice, and night marine air temperature since the late nineteenth century. *J. Geophys. Res.*, **108,** 4407, doi: 10.1029/2002JD002670

Ropelewski, C. F. and Jones, P. D. 1987 An extension of the Tahiti-Darwin Southern Oscillation Index. *Mon. Weather Rev.*, **115,** 2161–2165

Sivakumar, B., Berndtsson, R., Olsson, J., Jinno, K. and Kawamura, A. 2000 Dynamics of monthly rainfall-runoff process at the Göta basin: A search for chaos. *Hydrology and Earth System Sciences*, **4,** 407–417

Thompson, D. W. J. and Wallace, J. M. 1998 The Arctic Oscillation signature in the wintertime geopotential height and temperature fields. *Geophys. Res. Lett.*, **25,** 1297–1300
2000 Annular modes in the extratropical circulation. Part I: Month-to-month variability. *J. Climate*, **13,** 1000–1016

Thompson, D. W. J., Lee, S. and Baldwin, M. P. 2003 'Atmospheric processes governing the Northern Hemisphere Annular Mode/North Atlantic Oscillation.' Pp. 81–112 in *The North Atlantic Oscillation: Climatic Significance and Environmental Impact*. Eds. J. W. Hurrell, Y. Kushnir, G. Ottersen and M. Visbeck. *Geophysical Monograph*, **134**

Torrence, C. and Webster, P. J. 1999 Interdecadal changes in the ENSO–monsoon system. *J. Climate*, **12,** 2679–2690

Turner, J. 2004 The El Niño–Southern Oscillation and Antarctica. *Int. J. Climatol.*, **24,** 1–31

Vallis, G. K., Gerber, E. P., Kushner, P. J. and Cash, B. A. 2004 A mechanism and simple dynamical model of the North Atlantic Oscillation and annular modes. *J. Atmos. Sci.*, **61,** 264–280

Voss, R. and Mikolajewicz, U. 2001 Long-term climate changes due to increased CO2 concentration in the coupled atmosphere-ocean general circulation model ECHAM3/LSG. *Clim. Dyn.*, **17,** 45–60

Wang, C. 2005 'ENSO, Atlantic climate variability, and the Walker and Hadley circulations'. Pp. 173–202 in *The Hadley Circulation: Present, Past, and Future*. Eds. H. F. Diaz and R. S. Bradley. Kluwer Academic Publ., Netherlands

Wanner, H., Bronnimann, S., Casty, C., Gyalistras, D., Luterbacher, J., Schmutz, C., Stephenson, D. B. and Xoplaki, E. 2001 North Atlantic Oscillation—concepts and studies. *Surv. Geophys.*, **22,** 321–381

Wittman, M. A. H., Charlton, A. J. and Polvani, L. M. 2005 On the meridional structure of annular modes. *J. Climate*, **18,** 2119–2122